The Experimental Verification of the Lift, Thrust and Guidance Forces Created by an Electrodynamic Wheel Rotating Over a Split-Sheet Guideway

J. Bird & T. A. Lipo
University of Wisconsin-Madison, Madison, USA

ABSRACT: The rotation of radial positioned magnets above a split-sheet aluminum guideway induces currents in the guideway that can simultaneously create lift and thrust forces. The rotor is termed an electrodynamic wheel. Apart from the air-gap, the thrust forces are dependent on the difference between the circumferential velocity of the EDW and the translational velocity of the vehicle; at high translational velocity the lift force becomes predominantly independent of the circumferential velocity. Passive guidance forces result when the EDW is laterally off-centre from the split-sheet guideway while active guidance force can be produced by turning the EDW, as with an automobile. Preliminary experimental thrust, lift and guidance force results are presented and compared with 2D and 3D numerical models.

1 INTRODUCTION

High-speed maglev has many potential advantages over high-speed rail and short-haul aircraft (Lever 1998,Wahl 2004). However, despite these advantages its exorbitant capital cost has invariably resulted in countries choosing to upgrade or install high-speed rail, or solely depend on short-haul aircraft and highways. Therefore, based on its current implementation record, it appears that maglev will only ever achieve wider use if its construction costs can be greatly reduced. Such a large cost reduction is only achievable if the guideway is designed to be passive.

Passive maglev guideway designs were studied intensively in the 1970's and early 80's. The use of a single-sided linear induction motor (SLIM) with a track constructed of aluminum and back iron held early promise. But for high speed operation the SLIM suffers from a low power factor and it must be designed to be very long in order to counteract the end-effects (Eastham et al. 1987, Nonaka & Higuchi 1987). In addition, a secondary suspension system must be used which increases costs and creates drag losses (Borcherts & Davis 1974). When the SLIM track is constructed only of aluminum then the induced guideway currents will create a lift force, in addition to thrust. However, this 'electromagnetic river' concept (Eastham & Laithwaite 1974), has an abysmally low power factor (Katz et. al. 1979, Eastham & Rodger 1984), and the lift-to-weight ratio is low, thus its implementation has never been practically realized.

A passive reluctance type linear motor design, often called the Homopolar Iron Cored Linear Synchronous Motor (HICLSM) (Levi 1973, Boldea et. al. 1988, Cassat & Jufer 2002) has also been investigated for transportation. This motor uses a salient iron track under a girder, while the vehicle has a primary with an integrated traveling AC and DC excitation. The DC excitation provides an attractive lift force and magnetization field, while the AC winding's field is controlled so as to interact synchronously with the salient track, thereby creating propulsive force. As large eddy current drag forces will be induced in the track at high speed (Slemon 1979) the track iron needs to be laminated. Also, in order to prevent the iron from saturating the guideway iron must be made 1-2 times thicker than an equivalent SLIM guideway (Nondahl 1980, Eastham et. al. 1984), All these attributes result in this passive track design being significantly more costly than high-speed rail.

A third possibility is to mechanically rotate radial or axial positioned magnets over an aluminum guideway (Davis & Borcherts 1973, Borcherts & Davis 1979, Fuji et al. 1997, Bird & Lipo 2003, Bird & Lipo 2004). The rotation of the magnets enables a lift and thrust force to be created simultaneously via induced eddy currents. The radial magnet configuration is illustrated in Figure 1; such a configuration has been termed an electrodynamic wheel (EDW). As the magnets are inducing the guideway currents, the power factor is not affected and the rotation of the magnets results in the detrimental drag forces encountered in most electrodynamic suspension (EDS) and electromagnetic suspension (EMS) methods being converted into useful thrust (Bird & Lipo

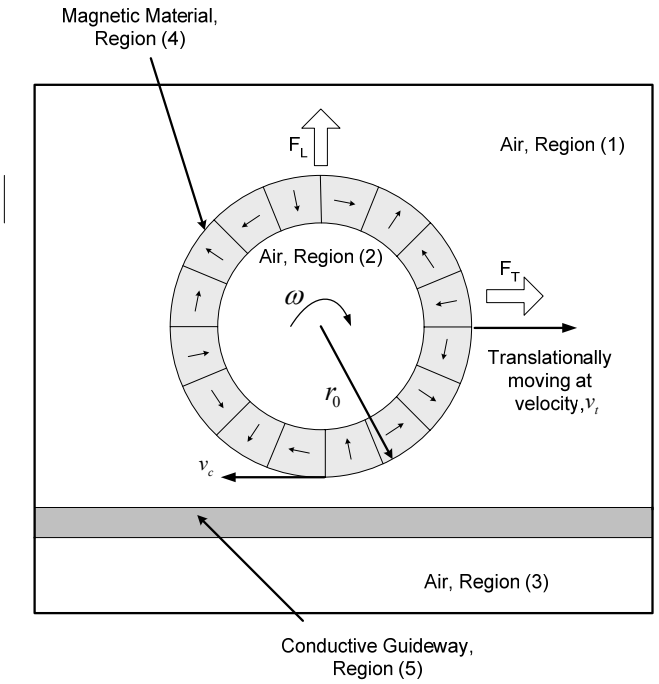

Figure 1: An Electrodynamic Wheel

2003). Although increased losses will result from the mechanical rotation, only one mechanism is needed to create the forces, thus reducing the overall losses.

The thrust force is created when the circumferential velocity, v_c, of the EDW becomes greater than the translational velocity, v_t. Thus, a slip, s, is always present:

$$s = v_c - v_t \tag{1}$$

$$= \omega r_o - v_t \tag{2}$$

where ω is the mechanical angular velocity and r_o is the rotor radius.

The use of this passive guideway topology could be relatively cheap as it is composed only of aluminum sheets and no girder is required. As there is little gained by suspending a vehicle at low speeds, it in envisaged that the vehicle will operate on wheels until it reaches a predetermined speed at which point sufficient lift and guidance forces will be naturally and actively created to enable stable suspension.

This paper presents preliminary experimental results of the force created using one 4 pole-pair NdFeB Halbach rotor rotated over a split-sheet aluminum guideway. Although using multiple EDWs in series would lead to better performance (Bird & Lipo 2005). This initial investigation is limited to using one EDW. The experimental results are compared with 2D and 3D numerical calculations, and a discussion on the reasons for discrepancies is given.

2 THE SPLIT-SHEET GUIDEWAY TOPOLOGY

The use of a horizontal flat passive maglev guideway is desirable for a number of reasons. First, the construction cost will be very low, since the guideway does not need to be elevated, as with EMS and the HICLSM, or use side-walls as with many EDL guideway configurations. Second, a flat guideway structure makes it possible to develop electromagnetic guideway directional switches, rather than having to use a mechanically moving guideway (Atherton & Eastham 1974, Raji 1977, He & Rote 1993). Third, a flat guideway could be more easily integrated into the existing transportation infrastructure. Fourth, flat structures are less likely to accumulate debris and snow. And fifth, flat guideway structures will create less aerodynamic drag forces (Barrows et. al. 1992). However an EDW above a single flat guideway, such as shown in Figure 2, is inherently unstable (Atherton & Eastham 1974, Ooi 1975, Atherton et al. 1978). This can be intuitively seen perhaps most easily by considering a ladder guideway rather than sheet, since the induced current paths will be analogous for this case. When a magnet is rapidly moved in a translational manner over a ladder guideway and is offset from the center, as illustrated in Figure 3, then induced currents are created that will force the magnet further off center. Thus, using any type of guideway with one sheet will create destabilization forces.

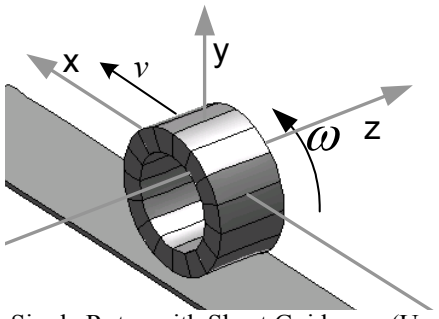

Figure 2: Single Rotor with Sheet Guideway (Unstable)

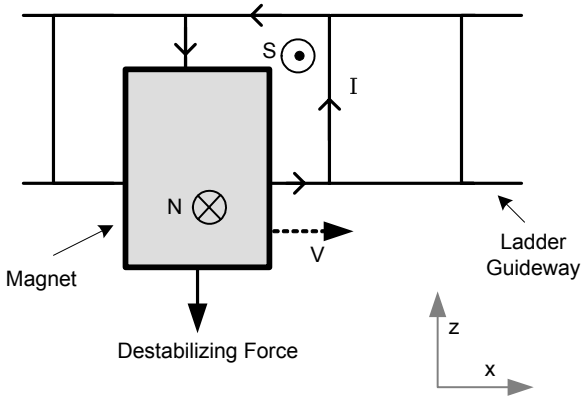

Figure 3: Illustration of the Induced Current Path Created when a Magnet is Translationally moving above a Ladder Guideway

In order to create electrodynamic stability the guideway must experience a net increase in the flux when the vehicle magnets are laterally displaced.

This will always occur when the guideway conductors see a minimum flux with respect to the vertical magnet field component when in an unperturbed state. For illustrative purposes, considering only the self-inductance, then the guideway electromagnetic energy in lumped-parameter form is simply:

$$E = \frac{1}{2} L i^2 \tag{3}$$

or, in terms of flux, Φ:

$$E = \frac{1}{2L} \Phi(x, y, z)^2 \tag{4}$$

The magnetic force acting on the guideway in the lateral z-direction can be obtained from the negative energy gradient: (Knoepfel 2000)

$$F_z = -\frac{\partial E}{\partial z} \tag{5}$$

Therefore from (4) and (5) one obtains:

$$F_z = -\frac{1}{L} \Phi \frac{\partial \Phi}{\partial z} \tag{6}$$

Assuming the vertical flux in the lateral direction is always positive then from (6) it is seen that the lateral force will only depend on the gradient of the flux with respect to the z-axis. Therefore, for the guideway topology shown in Figure 2 the flux, Φ, 'seen' by the guideway will be a maximum when the magnet is centered over the guideway and this will then give the energy profile, *E*, as a function of the lateral position, *z*, and the resulting lateral force, F_Z, as shown in Figure 4. Thus, confirming that stability can never be assured.

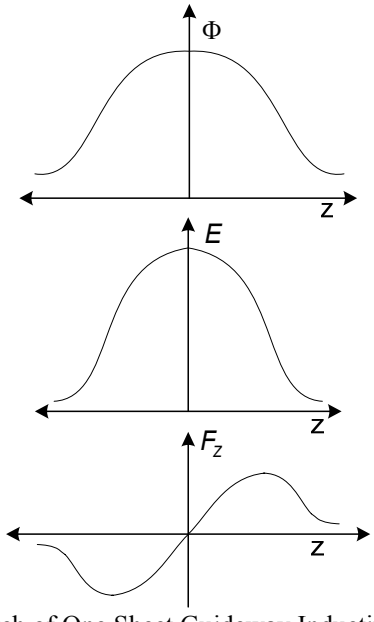

Figure 4: Sketch of One Sheet Guideway Inductive Energy and Unstable Lateral Force Profile

In order to create guidance it is proposed that a flat split-guideway conducting sheet topology be used. As illustrated in Figure 5. Such a guideway topology was previously proposed for translational EDL by Atherton and Eastham (Atherton & Eastham 1974,Howell et .al. 1975, Sakamoto et. al. 1991), and earlier by Kolm and Thornton in a curved configuration (Iwasa 1973,Kolm & Thronton 1973, Fang et al. 2004). An equivalent split-ladder guideway was proposed much later for translational EDL by He and Rote (He & Rote 1993). Such a configuration is advantageous because it can still create large lift and thrust or breaking forces while at the zero guidance position (center position). A sketch of the inductive energy and lateral force profile, as seen by one sheet of the guideway, for the split-sheet topology is shown in Figure 6.

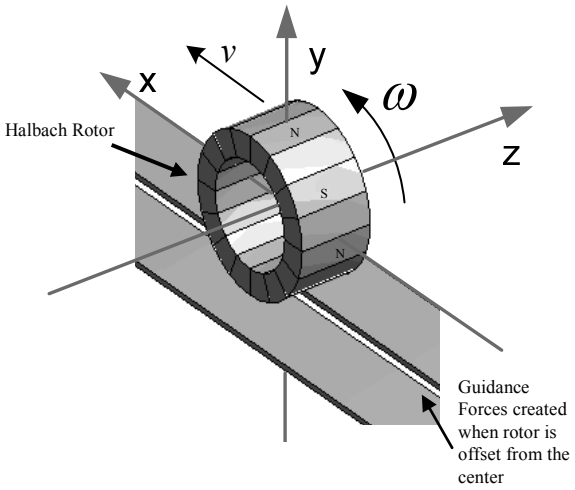

Figure 5: An Electrodynamic Wheel over a Split-Sheet Guideway.

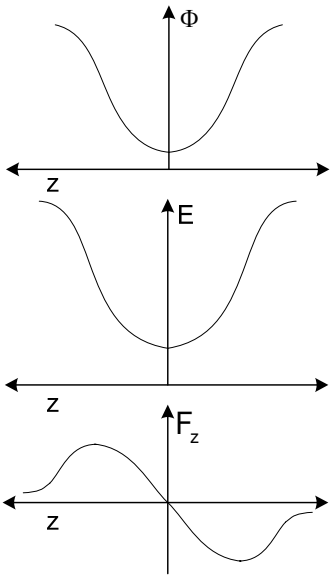

Figure 6: Inductive Energy and Stabilizing Lateral Force, 'Seen' by the Track, for the Split-Sheet Guideway Topology

The guidance forces can be generated in two ways, first passively by the fact that when the EDW is laterally off-center motional induced currents in the guideway will then be non-symmetric therefore creating a restorative force, and second active addi-

tional guidance forces can be created by turning the EDW around the y-axis, as illustrated in Figure 7. The turning of the EDW will create large additional guidance forces, but with a reduction in thrust.

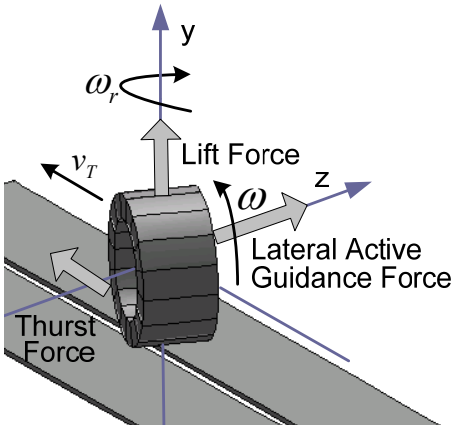

Figure 7: Additional Active Lateral Guidance Forces Are Created by Rotating the EDW about the y-Axis

3 EXPERIMENTAL REALIZATION

In order to validate the predicted forces (Bird & Lipo 2004, Bird & Lipo 2005) an experimental EDW driven 'vehicle' has been constructed. For measurement convenience the 'vehicle' is held stationary while the guideway moves. This was achieved by using a 1.2m diameter wheel with two 77mm aluminum sheets separated by 2mm to represent the guideway. The EDW was rotated above this guideway wheel. The complete experimental set-up, showing the guideway wheel and 'vehicle' above the guideway wheel is shown in Figure 8. The induction machine and controller in the foreground are used only for breaking purposes so as to enable the guideway to be held at a constant speed while making measurements.

3.1 Halbach Rotor

In order to attain the highest possible lift-to-weight ratio a 4-pole-pair NbFeB Halbach rotor was used with a 2D optimized magnet thickness (Bird & Lipo 2004). The calculated 2D field lines for the Halbach rotor are illustrated in Figure 9. More detailed rotor (and guideway) parameters are shown in Table 1. The constructed 50mm radii Halbach rotor is shown in Figure 10. The rotor yoke and part of the sleeve are Lexan, also an additional 0.6mm Kevlar thread was added to the sleeve. Rather than designing an integrated motor to drive the EDW two brushless DC motors on either side of the rotor have been used.

The predicted x and y magnetic field density components at z = 0 for the Halbach rotor based on 2D FEA, 3D FEA and a 3D analytic model (Bird & Lipo 2005) are compared with the experimentally measured results in Figure 11 and 12. The 3D FEA results are sporadic due to the limitation on element size. The experimental field value is approximately 10% lower than the predicted value. The peak field value reduces near the edges of the rotor, as illustrated in Figure 13. This field reduction results in a reduced force compared with the predicted 2D model. Also the z-field component, not present in the 2D model, becomes a maximum near the magnet rotor edge, as shown in Figure 14.

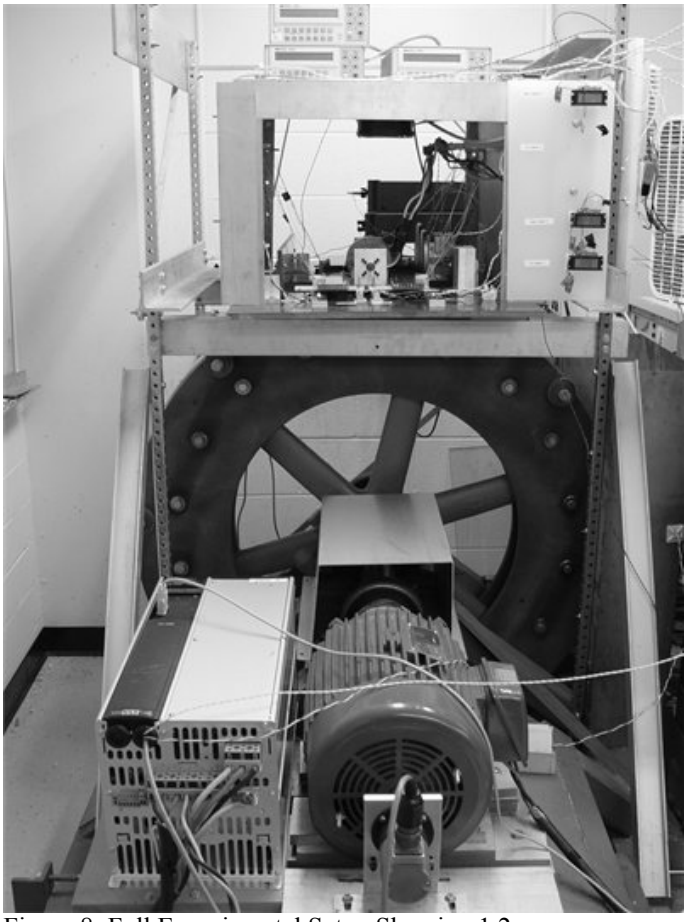

Figure 8: Full Experimental Setup Showing 1.2m Diameter Split-Sheet Guideway Wheel

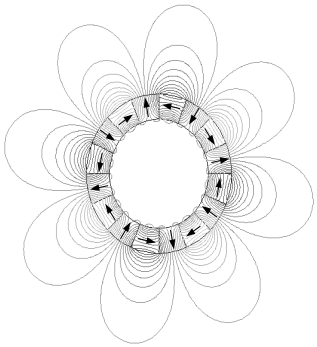

Figure 9: Field Lines for a 4 Pole-Pair Halbach Rotor

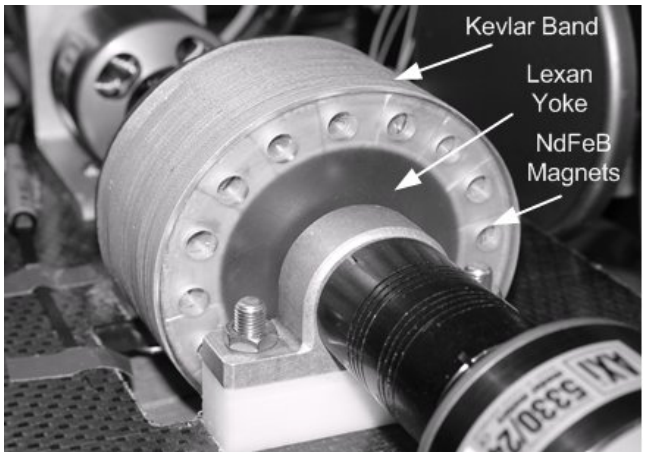

Figure 10: Experimental Realisation of the 4 Pole-Pair Halbach Rotor (shown between brushless DC driving motors)

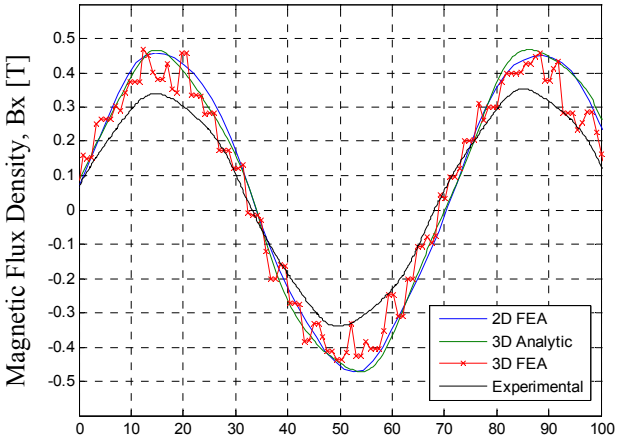

Figure 11: Bx Field Comparison 7mm from Rotor, at z=0

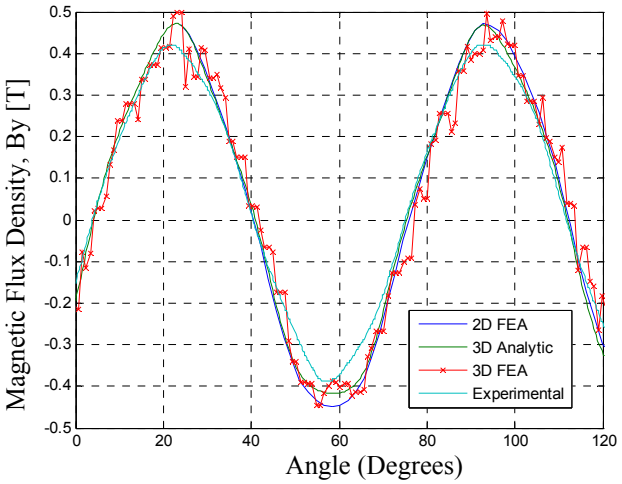

Figure 12: By Field Comparison, 7mm from Rotor, at z=0

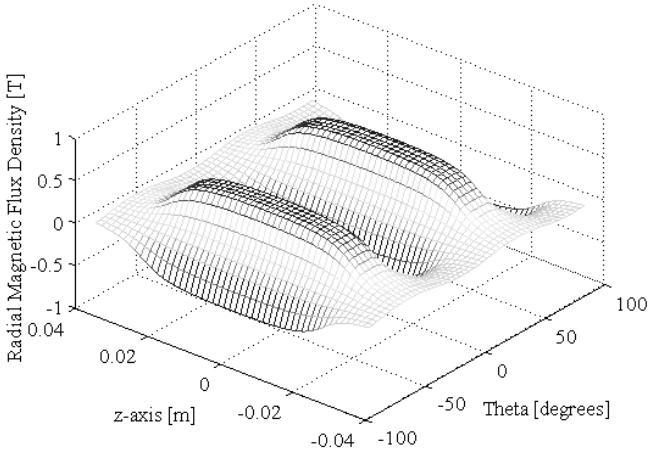

Figure 13: Analytically Calculated Radial Flux Density Component, Br, 5mm from the Rotor Surface for 4 of the Poles

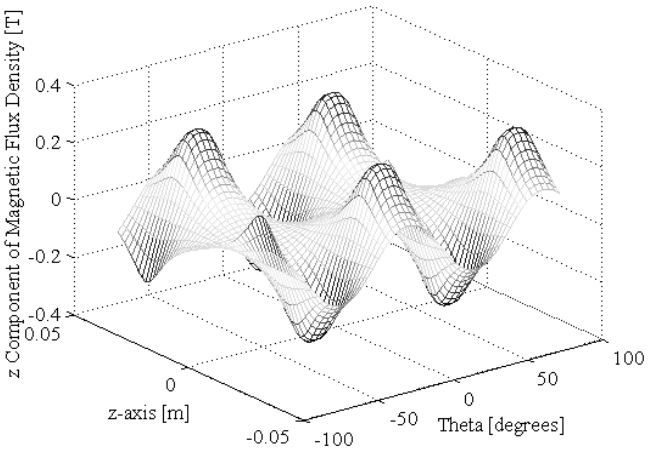

Figure 14: Analytically Calculated Lateral Flux Density Component, Bz, 5mm from the Rotor Surface for 4 of the Poles

3.2 Experimental Force Measurements

For testing purposes, the airgap for this scale model has initially been set large (11.7mm) so as to limit the forces. The lift force was measured by measuring the reduction in vehicle's mass via four load cells placed below each corner of the 'vehicle', two of which are shown at the bottom of Figure 15. The thrust force was measured by two load cells that the 'vehicle' pushes against, shown at the front of the 'vehicle'. Also four small moveable lateral guidance force sensors have been used. Two of which are shown in Figure 15. The lateral force was measured when the 'vehicle' and the sensor pushes on the white plastic stops affixed to the four corners of the 'vehicle'. The two brushless DC drive motors are also clearly shown in the figure. The vehicle's carbon fiber base is free to slide on the lift sensors and between the guidance and thrust sensors.

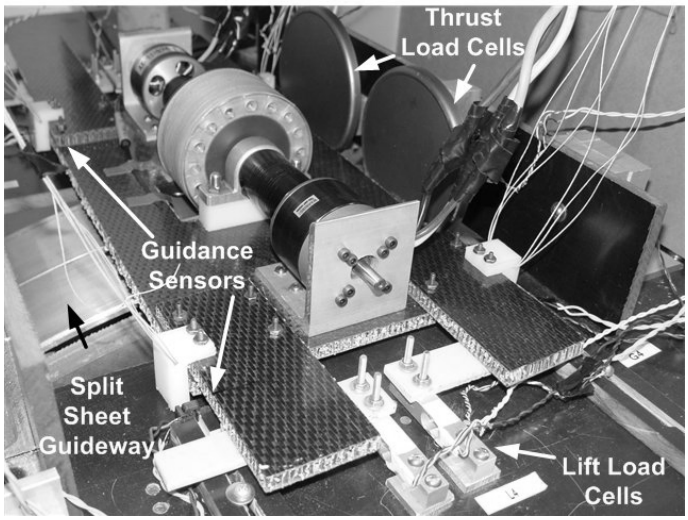

Figure 15: Test 'Vehicle' above Split-Sheet Guideway Wheel

Table 1: Experimental Parameters			
Rotor:	Magnet Outer Radius	50	mm
	Inner radius	34.2	mm
	Width	50	mm
	Magnet (NdFeB), B_r	1.42	T
	Pole Pairs	4	
	Sleeve thickness	2.6	mm
Guideway:	Radius	600	mm
	Conductivity (Al)	2.459×10^7	Sm^{-1}
	Single Sheet Width	77	mm
	Split Sheet Gap	2	mm
	Thickness	6.3	mm
	Electrical Airgap	11.7	mm
	Mecahnical Airgap	9.1	mm
'Vehicle Mass'		4.7	kg

4 COMPARISON WITH 2D STEADY-STATE CURRENT SHEET MODEL

In order to experimentally validate the 2D steady state equivalent current sheet model of the EDW (Bird & Lipo 2004) the EDW was first rotated completely over just one side of the split-sheet guideway.

After comparing the 2D steady-state models predicted forces with a transient Magsoft Flux 3D model (with no translational motion) it was determined, as expected, that the 2D model overestimates the forces. The main cause for this discrepancy is due to the magnitude of the radial (and azimuthal) field along the z-axis reducing, as shown in Figure 13, thereby reducing the force. Additional minor reductions in force are due to the finite track width and the track curvature; their exact effect is dependent on the air-gap.

An example of the difference between the predicted 2D and 3D results is shown in Figure 16 and 17. The Magsoft Flux 3D FEA results for a flat track, a curved track and the 2D steady-state force results at various RPM, but with no translational motion, are compared. In this comparison an 8 mm air-gap was used. The comparison shows that the 2D results are approximately 30% greater. An example, of the meshed geometry, used for the 3D curved track model, is shown in Figure 18.

A further cause for discrepancy between the 2D and 3D models is due to the presence of the B_z component in the lift force calculation. The z-component of the rotor field becomes relatively large near the rotor edges, as shown in Figure 14, and this leads to the 3D calculated Lorentz force being different. Since in 3D the Lorentz force is:

$$F_x = \iiint_V (J_y B_z - J_z B_y) dV \quad \text{Thrust Force} \tag{7}$$

$$F_y = \iiint_V (J_x B_z - J_z B_x) dV \quad \text{Lift Force} \tag{8}$$

$$F_z = \iiint_V (J_x B_y - J_y B_x) dV \quad \text{Guidance Force} \tag{9}$$

where the integral is evaluated over the guideway volume, V. As the J_y term in (7) and (9) is negligible only the lift force will be affected by the B_z term.

Using these comparisons it was determined that the 2D field should be reduced by 16% in order to more closely account for the above mentioned 3D effects. After accounting for this and also the reduction in peak field magnitude compared with the experimental measurements the experimental and predicted 2D steady-state FEA model results agreed well at low slip values. A comparison between the experimental and 2D steady-state model is shown in Figure 19 and 20 for 8m/s and 12m/s translational velocities (at an 11.7mm air-gap). Note how the experimental and calculated thrust and lift force results intersect at the same slip value, thus confirming that the geometric and material parameters are correct. Also, as expected, the lift force does not go to zero at zero slip because of the translational motion. The discrepancy between the empirical and calculated values at higher slip is perhaps due to the uneven air-gap close to lift-off speed, and due to the increase in guideway temperature (lowering the aluminum conductivity). The guideway being out-of-round by over 0.2mm will also cause some discrepancies.

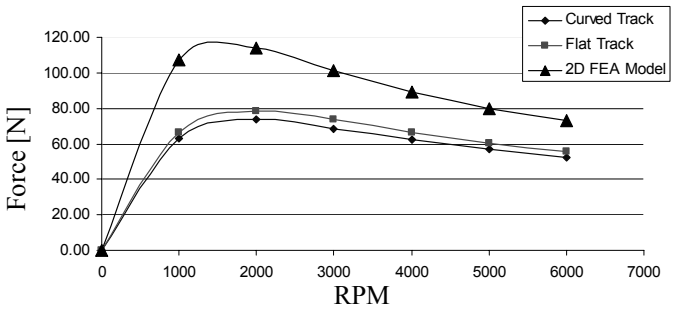

Figure 16: Thrust Force Comparison between 2D Steady-state FEA Model and 3D Models (no translational motion)

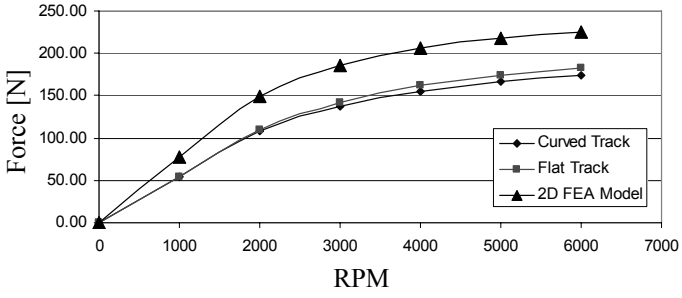

Figure 17: Lift Force Comparison between 2D Steady-state FEA Model and 3D Models (no translational motion)

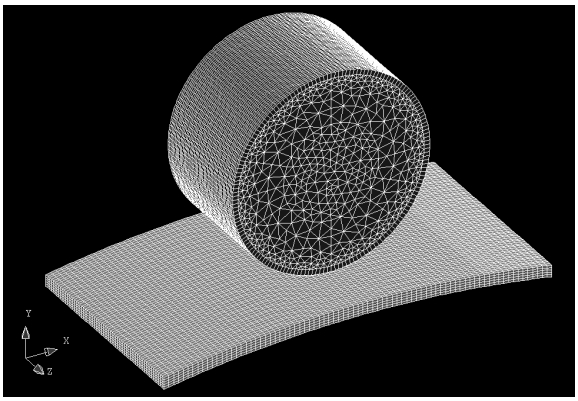

Figure 18: Meshed Rotor with a Single Curved Sheet Guideway

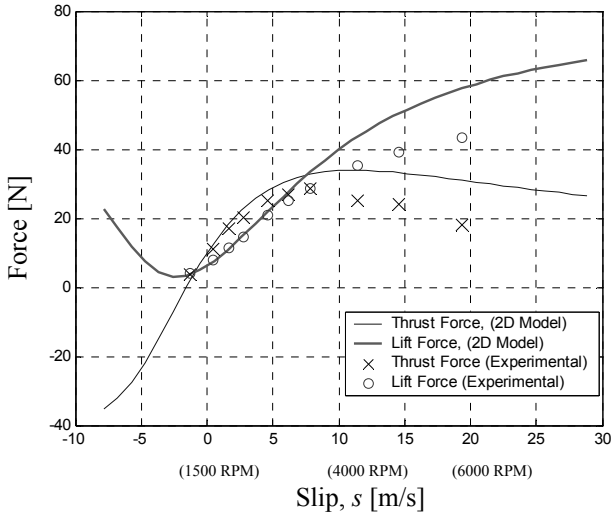

Figure 19: Thrust and Lift Force Comparison at an 8 m/s Translational Velocity

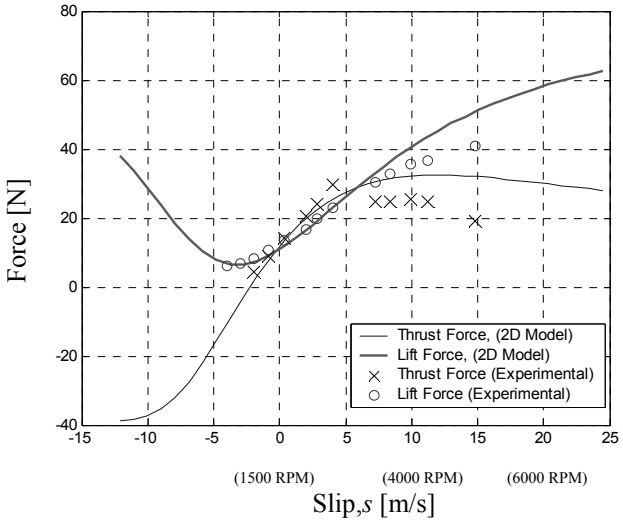

Figure 20: Thrust and Lift Force Comparison at a 12 m/s Translational Velocity

5 GUIDANCE FORCE COMPARISON WITH 3D TRANSIENT FINITE ELEMENT MODEL

It has been noted that passive guidance forces are generated when the vehicle is laterally off-center. In order to compare the guidance force creation with the split-sheet Magsoft Flux 3D model, shown in Figure 21, the guideway wheel was prevented from rotating and the forces were measured for a range of EDW rotational speeds. The force comparison at 2500RPM for a number of lateral offset positions is shown in Figure 22. The results show a general agreement. The measured guidance forces are somewhat larger than expected and this is partly due to the friction force being a larger percentage of the total guidance force. Lastly, Figure 23 shows the raw experimental data obtained for the case when there is a 10m/s translational speed and the EDW is laterally offset from the center by 12mm. The results tend to show that like with the thrust force there is a peak guidance force value at a particular slip. Additional guidance and experimental results will be presented in the oral presentation.

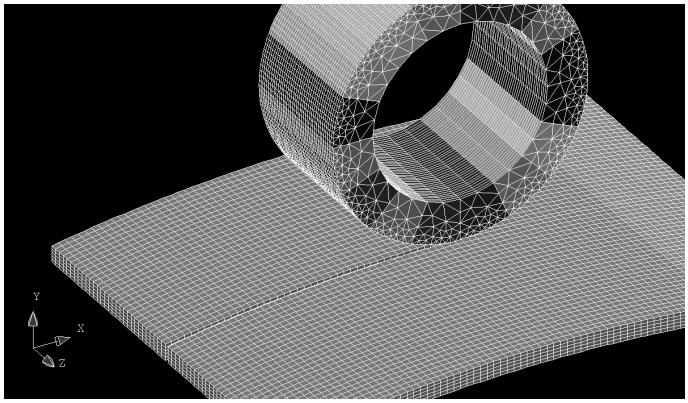

Figure 21: Meshed Rotor with Split-Sheet Aluminum Guideway

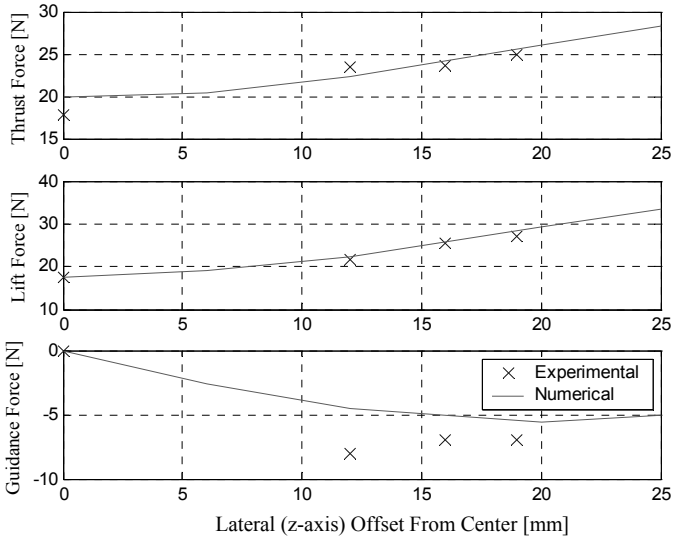

Figure 22: Steady-State Lift, Thrust and Guidance Force Comparison at 2500 RPM, 0 m/s Translational Speed with an 11.7mm Air-Gap

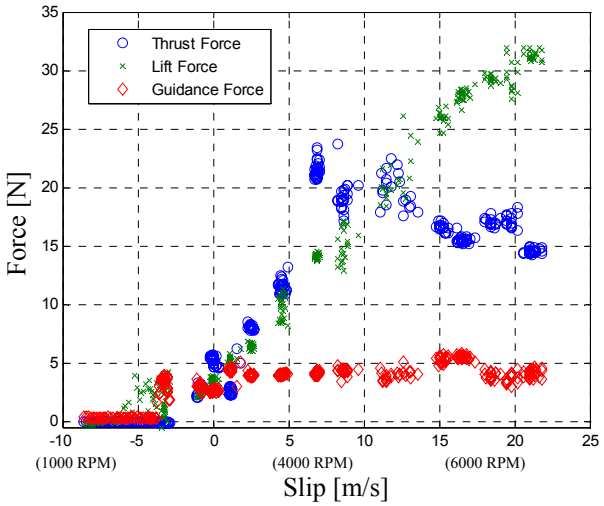

Figure 23: Example of Raw Experimental Results for the Thrust, Lift and Guidance Forces with a Guideway Translational Velocity of 10m/s (36 km/h) and Offset by 12 mm

6 CONCLUSIONS

Preliminary experimental results, using a large air gap with low guideway speeds have been presented. The results confirm that the experimental setup is capable of measuring the simultaneously created lift, thrust and guidance forces for an EDW using a split-sheet aluminum guideway. The initial results and the 3D transient FEA model (with no translation) confirm that a full 3D analysis is required in order to properly optimize and design an EDW driven maglev system. The effect of the magnet width, track width and force relationships created by the split-sheet guideway need to be further characterized.

If the field values are scaled correctly, the 2D steady-state current sheet model is capable of predicting the thrust and lift force relationships with reasonable accurately.

This type of maglev technology, using either rare-earth or superconducting magnets, is complex to design and control. However, it appears that this maglev system is worthy of further investigation since the use of electrodynamic wheels will enable the guideway to be very low cost and therefore, perhaps, enable maglev to successfully compete with and complement other modes of transportation.

7 ACKNOWLEDGEMENTS

The authors would like to acknowledge the support provided by the member companies of the Wisconsin Electric Machines and Power Electronics Consortium (WEMPEC) at the University of Wisconsin-Madison. Also the authors would like to thank Shingo Kato at Honda R&D for assisting with the construction of the experimental setup, Dr J. Hull at Argonne National Laboratories for providing the guideway wheel and the Magsoft Corporation for the use of their Flux 3D FEA software.

8 REFERENCES

Atherton, D.L. & Eastham, A.R. 1974. Flat guidance schemes for magnetically levitated high-speed guided ground transport. *J. Appl. Phys.* 45(3): 1398-1405.

Atherton, D.L., et al. 1978. Forces and moments for electrodynamic levitation systems - large-scale test results and theory. *IEEE Trans. Magn.* 14(2): 59-68.

Barrows, T., et al. 1992. *Aerodynamic Forces on Maglev Vehicles*, U.S. Department of Transportation, DOT/FRA/NMI-92/21

Bird, J. & Lipo, T.A. 2003. An electrodynamic wheel: an integrated propulsion and levitation machine. *IEMDC* 3: 1410-1416.

Bird, J. & Lipo, T.A. 2004. *A preliminary investigation of an electrodynamic wheel for simultaneously creating levitation and propulsion*. 18th Intern. Conf. on Magnetically Levitated Systems and Linear Drives, Shanghai, China.

Bird, J. & Lipo, T.A. 2005. *Electrodynamic wheel and flat passive track topologies capable of creating lift, thrust and guidance forces simultaneously*. 8th Intern. Symp. On Magnetic Suspension Technology, Dresden, Germany.

Bird, J. & Lipo, T.A. 2005. *A study of the effect of using electrodynamic wheels in series*. 8th Intern. Symp. On Magnetic Suspension Technology, Dresden, Germany.

Boldea, I., et al. 1988. Field tests on a maglev with passive guideway linear inductor motor transportation system. *IEEE T. Veh. Tenchol* 37(4): 213-219.

Borcherts, R.H. & Davis, L.C. 1974. Lift and drag forces for the attractive electromagnetic suspension systems. *IEEE Trans. Magn.* 10(3): 425-428.

Borcherts, R.H. & Davis, L.C. 1979. The superconducting paddlewheel as an integrated propulsion levitation machine for high speed ground transportation. *Electr. Mach. Electrom.* 3: 341-355.

Cassat, A. & Jufer, M. 2002. MAGLEV projects technology aspects and choices. *IEEE T. Appl. Supercon.* 12(1): 915-925.

Davis, L.C. & Borcherts, R.H. 1973. Superconducting paddle wheels, screws, and other propulsion units for high-speed ground transportation. *J. Appl. Phys.* 44(7): 3294-3299.

Eastham, J.F., et al. 1984. *A comparison of some propulsion methods for magnetically-levitated vehicles*. Maglev Transport Now and for the Future, Solihull England.

Eastham, J.F., et al. 1987. Comparison of short primary linear machines for high speed maglev vehicles. *IEEE Trans. Magn.* 23(5): 2338-2343.

Eastham, J.F. & Laithwaite, E.R. 1974. Linear induction motors as 'electromagnetic rivers'. *Proc. IEE* 121(10): 1099-1108.

Eastham, J.F. & Rodger, D. 1984. The performance of induction levitators. *IEEE Trans. Magn.* 20(5): 1684-1686.

Fang, J., et al. 2004. *Dynamic modeling and control of the magplane vehicle*. 18th Intern. Conf. on Magnetically Levitated Systems and Linear Drives, Shanghai, China.

Fujii, N., et al. 1997. Three dimensional force of magnet wheel with revolving permanent magnets. *IEEE Trans. Magn.* 33(5): 4221-4223.

He, J.L. & Rote, D.M. 1993. Double-row loop-coil configuration for EDS maglev suspension, guidance, and electromagnetic guideway directional switching. *IEEE Trans. Magn.* 29(6): 2956-2958.

Howell, J.P., et al. 1975. Stability of magnetically levitated vehicle over a split guideway. *IEEE Trans. Magn.* 11(5): 1487-1489.

Iwasa, Y. 1973. Electromagnetic flight stability by model impedance simulation. *J. Appl. Phys.* 44(2): 858-862.

Katz, R.M., et al. 1979. Integrated magnetic suspension and propulsion of guided ground transportation vehicles with a SLIM. *IEEE Trans. Magn.* 15(6): 1437-1439.

Knoepfel, H.E. 2000. *Magnetic fields: A Comprehensive Theoretical Treatise for Practical Use*. New York, John Wiley & Sons.

Kolm, H.H. & Thronton, R.D. 1973. Electromagnetic flight. *Scientific American* 229(4): 17-25.

Lever, H.J. 1998. *Technical Assessment of Maglev System Concepts, Final Report by the Government Maglev System Assessment Team*, US Army, CRREL-SR-98-12

Levi, E. 1973. Linear synchronous motors for high-speed ground transportation. *IEEE Trans. Magn.* 9(3): 242-248.

Nonaka, S. & Higuchi, T. 1987. *Design strategies of single-sided linear induction motors for propulsion of Vehicles*. Intern. Conf. on Maglev and Linear Drives, Las Vegas.

Nondahl, T.A. 1980. Design studies for single-sided linear electric motors: homopolar synchronous and induction. *Electr. Mach. Electrom.* 5: 1-14.

Ooi, B.T. 1975. Transverse force in magnetic levitation with finite width sheet guideways. *IEEE Trans. on Power Apparatus and Systems* 94(3): 994-1002.

Raji, A.G. 1977. *A Nonlinear Model for a Maglev Vehicle*. Electrical Engineering, McGill University, Montreal, Canada

Sakamoto, T., et al. 1991. Induced currents and forces for the split-guideway electrodynamic levitation system. *IEEE Trans. Magn.* 27(6): 5004-5006.

Slemon, G.R. 1979. An experimental study of a homopolar linear synchronous motor. *Electr. Mach. Electrom.* 4: 59-70.

Wahl, G. 2004. *The maglev system transrapid - a future-oriented technology for track-bound transportation systems*. 18th Intern. Conf. on Magnetically Levitated Systems and Linear Drives, Shanghai, China.